Organic LETTERS

Letter

pubs.acs.org/OrgLett

Enantioselective Alkylation by Binaphthyl Chiral Phase-Transfer Catalysts: A DFT-Based Conformational Analysis

Takashi Kamachi and Kazunari Yoshizawa*

Institute for Materials Chemistry and Engineering and International Research Center for Molecular Systems, Kyushu University, Fukuoka 819-0395, Japan

Supporting Information

ABSTRACT: A conformational search method based on the density functional theory (DFT) was successfully applied to explore a mechanism for the highly enantioselective alkylation by binaphthyl-modifed chiral phase-transfer catalysts. Key interactions that govern the enantioselectivity were analyzed. The computational results are encouraging for further application of the DFT-based conformational search toward the rational design of next-generation asymmetric phase transfer catalysts.

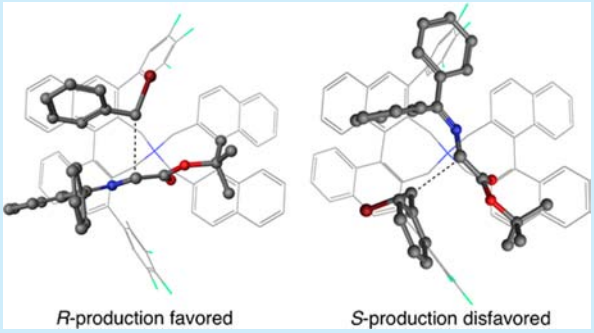

Asymmetric organocatalysis is one of the most useful methods for a wide variety of enantioselective transformations. Among them, asymmetric phase-transfer catalysis using chiral quaternary ammonium salts such as cinchona alkaloid and binaphthyl derivatives has advanced dramatically because of its simple experimental procedure, mild reaction conditions, and the environmentally benign nature of the reaction system.[1−4] In particular, chiral *N*-spiro quaternary ammonium salts bearing two different binaphthyl-modified subunits **1**, which are now commercially available as a "Maruoka catalyst", were successfully applied to various asymmetric phase-transfer reactions (Scheme 1).[5−8]

The phase-transfer benzylation of **2** with (*S*,*S*)-**1** and (*R*,*R*)-**1** proceeds smoothly at 0 °C to give the corresponding benzylation product with excellent enantioselectivity. The introduction of aromatic substituents at the 3,3′-position of one binaphthyl subunit is crucial to obtain excellent enantioselectivity.[9] As shown in Figure 1, the alkylation begins

Scheme 1. Asymmetric Benzylation of Glycine Derivatives 2 with Maruoka Catalysts

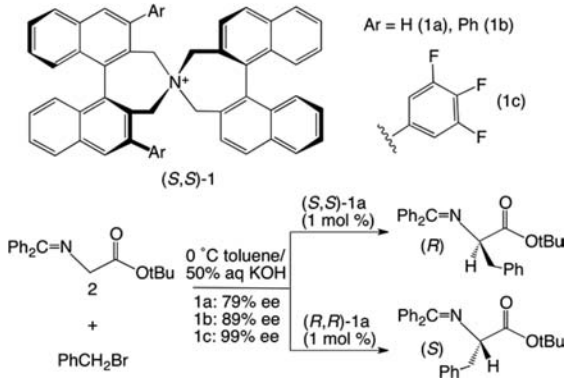

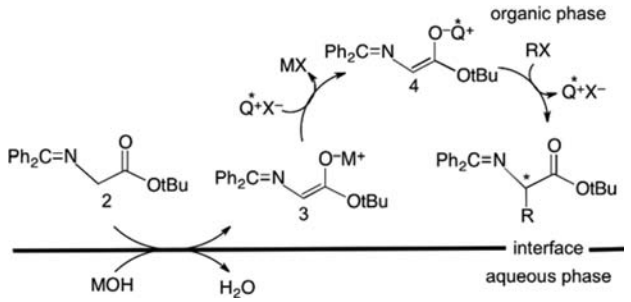

Figure 1. General mechanism for the asymmetric alkylation of **2** with the Maruoka catalyst (Q^+).

with the interfacial deprotonation of the α-proton of **2** to give enolate ion **3**. The enolate molecule binds to the catalyst by weak interactions, leading to noncovalent catalyst−enolate complex **4**. This complex reacts with an alkyl halide molecule to give an optically active monoalkylation product. In this letter, we present the first systematic DFT-based conformation analysis of the catalyst to reveal the origin of the excellent enantioselectivity.

To determine the lowest-energy transition structures leading to *R*- and *S*-products, we performed a DFT-based conformation search of the transition state for the nucleophilic attack of the enolate ion to benzyl bromide in the presence of (*S*,*S*)-**1c**. Initial structures of the transition state were generated with a

Received: November 19, 2013
Published: December 18, 2013

dx.doi.org/10.1021/ol4033545 | *Org. Lett.* 2014, 16, 472−475

conventional molecular mechanics based conformational search using the MacroModel program.[10] Two isoenergetic diastereomers of the enolate ion were considered in the conformational search (Figure S1). A total of 1436 initial conformations were obtained when all conformations within 20 kcal/mol above the global minimum were considered. The OPLS 2005 force field[11] was used for the calculations. The obtained structures were reoptimized by using the PM6-DH+ semiempirical method[12] implemented in the MOPAC program.[13] This method was parametrized to include dispersion and hydrogen-bonding corrections for describing weak interactions correctly at low computational cost. Then, we optimized 154 refined structures whose MOPAC energy is within 10 kcal/mol above the global minimum using the B97-D functional[14] and the resolution of identity approximation[15,16] implemented in the Turbomole program.[17] This is one of the most accurate DFT methods with dispersion correction to yield structures and interaction energies for a wide variety of noncovalent complexes including large van der Waals systems.[14] We used the SV(P)[18] basis set on all the atoms. The C···C distance between the α-carbon of the enolate ion and the benzylic carbon of benzyl bromide was fixed to 2.7 Å in the MacroModel, MOPAC, and DFT calculations to generate a reasonable initial guess for subsequent transition state searches. As summarized in Table S1, the top 20 conformations of the partially optimized structures account for 100.0% population, and they are fully optimized to locate the transition states. We used the TZVP[19] basis set on all the atoms for the transition state search. Finally 18 discrete conformations of the transition state were obtained.

Table 1 summarizes computed energies and Boltzmann populations of the lowest 10 conformations of the transition state. The top three conformations of the transition state give the *R*-product and accounts for the 99.9% population, which is in excellent agreement with the observed enantioselectivity of the catalyst. The energy difference between the most stable conformation for the *R*- and *S*-production (#1 and #4) is 5.3 kcal/mol. To assess the ability of the B97-D method for describing weak interactions in the system, we re-evaluated the energy difference with three other methods, B3LYP-D,[20−22] RI-MP2,[23] and RI-CC2.[24] As summarized in Table S2, these methods also give a large energy difference, and therefore, our conclusion is not influenced by the methods chosen here. As depicted in Figure S2, the top three conformations are similar in their structures, and we focus on the most stable conformation (#1) of the transition state to reveal key factors for the high enantioselectivity.

Table 1. Lowest 10 Conformations of the Transition State with Boltzmann Populations (%) at 0 °C on the Basis of DFT Energies (kcal/mol)

conf.	energy	population	chirality
1	0.0	91.5	*R*
2	1.3	7.9	*R*
3	2.8	5.4×10^{-1}	*R*
4	5.3	5.5×10^{-3}	*S*
5	7.2	1.4×10^{-4}	*R*
6	9.1	4.5×10^{-6}	*R*
7	9.5	2.4×10^{-6}	*S*
8	11.0	1.4×10^{-7}	*S*
9	12.2	1.5×10^{-8}	*S*
10	12.3	1.4×10^{-8}	*S*

Figure 2 shows top and side views of the most stable conformation of the transition state. In the transition state, the benzylation occurs via the nucleophilic attack of the *Re*-face of the enolate ion in the vicinity of the cationic ammonium center. The C−Br and C−C bond distances are 2.258 (2.383) and 2.977 (2.665) Å at the B97-D (B3LYP-D) level of theory, respectively. Let us first look at key interactions in the transition state to understand why this conformation is the most stable. Figure 3a shows the charge distribution in the transition state for the benzylation at the RI-B97-D/TZVP level of theory. The total charge of the transition state is −1, the negative charge being localized on the leaving Br atom and the carbonyl oxygen in addition to the α-carbon. To stabilize the transition state, the negatively charged atoms come into close contact with the cationic ammonium center of the catalyst. As shown in Figure 3b, the anionic atoms form hydrogen bonds to the α-hydrogens of the ammonium moiety in the most stable conformation. Table S3 lists the distances from the spiro N atom to the Br atom and to the carbonyl oxygen. The relative energy of the conformations increases as the N···Br and N···O distances increase and the maximum Coulombic interactions are achieved in the most stable conformation. These results show that the Coulombic interactions would be the main factor in controlling the conformation of the transition state.

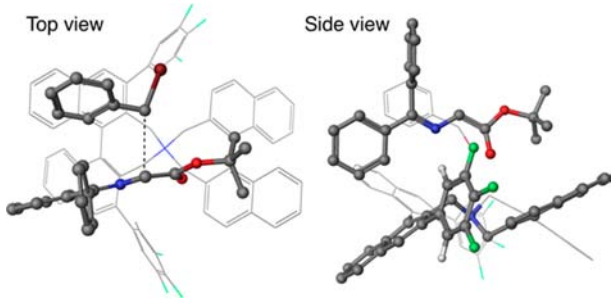

Figure 2. Top and side views of the most stable conformation (#1) of the transition state leading to the *R*-product in the benzylation. The near side is displayed in a ball-and-stick style. Gray, C; blue, N; red, O; green, F; and brown, Br.

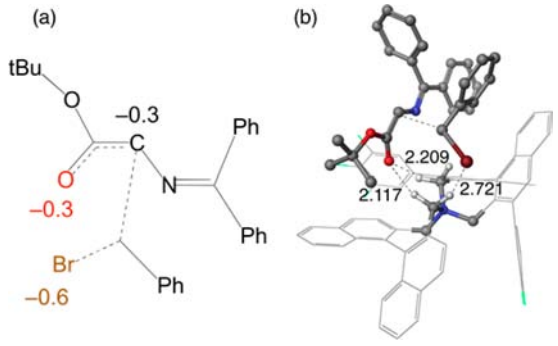

Figure 3. (a) Atomic charge distribution in the transition state for the benzylation. (b) Coulombic interactions between the anionic atoms in the transition state and the cationic ammonium center. Important parts are displayed in a ball-and-stick style. Units in Å.

Maruoka and co-workers[25] synthesized (*S*,*S*)-**2** having two equivalent binaphthyl-modified subunits and monoaryl sub-

dx.doi.org/10.1021/ol4033545 | *Org. Lett.* 2014, 16, 472−475

stituted (*S*,*S*)-**3** to investigate the effects of the aromatic substituents (Scheme 2). These catalysts exhibit a slightly lower

Scheme 2. Two Equivalent Binaphthyl-Modified (Left) and Monoaryl Substituted (Right) Maruoka Catalysts

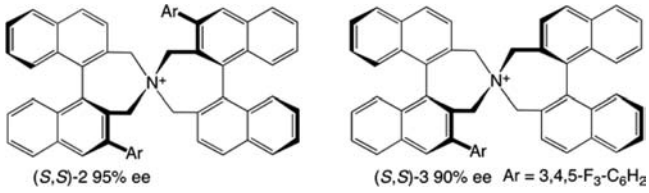

enantioselectivity (95% ee for (*S*,*S*)-**2** and 90% ee for (*S*,*S*)-**3**) in comparison with (*S*,*S*)-**1c**, but both catalysts show much higher enantioselectivity than nonaryl substituted (*S*,*S*)-**1a** (79% ee). These experimental findings indicate the existence of secondary interaction between the substituents and the enolate ion. In the most stable conformation, the 3,4,5-trifluorophenyl groups of the catalyst form nonclassical hydrogen bonds to the leaving Br atom and to the N atom of the enolate ion, which shows that the identity of the secondary interaction is likely to be the hydrogen bonds (Figure 4). The negatively charged Br

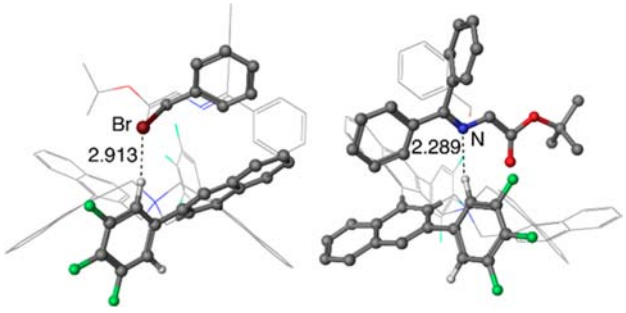

Figure 4. Nonclassical hydrogen bonds (C−H···X, X = Br and N) donated by the 3,4,5-trifluorophenyl groups of the catalyst in the most stable conformation. Units in Å.

atom and, to a lesser extent, the N atom are stabilized by the hydrogen bonds. The weaker C−H···N interaction would be lost in the catalysis of (*S*,*S*)-**2** and (*S*,*S*)-**3**, leading to the slight reduction of the enantioselectivity. The F atoms at the 3,4,5-postions of the substituent play a critical role in the enantioselectivity; (*S*,*S*)-**1b** shows a lower enantioselectivity of 89% ee. This is because the acidity of the H atom at the 2,6-positions of the substitutent is increased by the F atoms to strengthen the hydrogen-bonding interactions.

With the information on the key interactions in mind, we attempt to understand why the high enantioselective benzylation takes place in the presence of (*S*,*S*)-**1c**. Figure 5a shows an imaginary conformation for the *S*-production where the benzylation occurs via the nucleophilic attack of the *Si*-face of the enolate ion. We manually placed the benzyl bromide and the enolate ion, so that the anionic Br and carbonyl oxygen would have maximum interactions with the ammonium center and substituents in a similar manner to the most stable conformation for the *R*-production. However, the benzyl bromide and the enolate ion rotate approximately 45° around the ammonium center in the most stable actual conformation (#4) for the *S*-production, as shown in Figure 5b. The C−Br and C−C bond distances are 2.444 (2.462) and 2.689 (2.544) Å at the B97-D (B3LYP-D) level of theory, respectively. In the

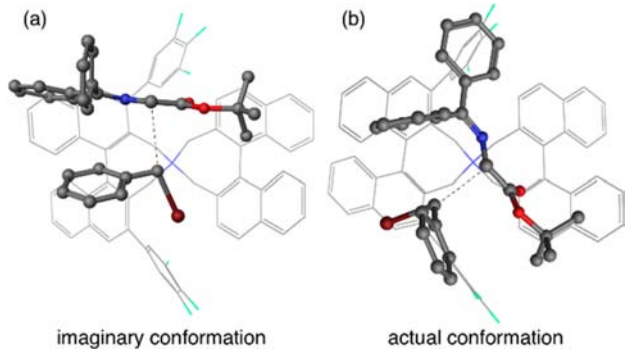

Figure 5. (a) Imaginary conformation for the transition state leading to the *S*-product. (b) The most stable actual conformation (#4).

actual structure, the N···Br distance is much longer than that in the most stable transition state for the *R*-production and the C−H···N interaction is lost, and therefore, the *S*-production is disfavored. Figure 6 shows a side view from a different angle of

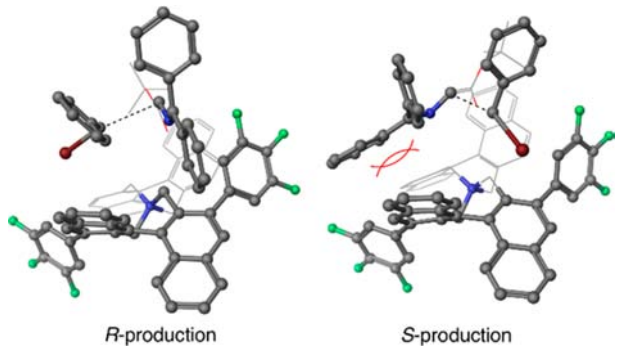

Figure 6. Side view from a different angle of the most stable conformation of the transition state leading to the *R*- and *S*-products.

the most stable conformation of the transition state for the *R*- and *S*-production. A phenyl group of the enolate ion experiences a significant steric interaction with the binaphthyl subunit of the catalyst in the transition state for the *S*-production, whereas the repulsion is not observed in the case of the *R*-production due to the asymmetric geometry of the binaphthyl subunit. To avoid the steric interaction, the enolate ion rotates as shown in the actual conformation for the *S*-production, leading to the loss of some key interactions between the reactants and the catalyst.

In summary, we performed a DFT-based conformation search to determine the lowest-energy transition structures leading to *R*- and *S*-products in the highly enantioselective benzylation by binaphthyl-modifed chiral phase-transfer catalysts. In the most stable conformation for the *R*-production, the negatively charged Br atom and carbonyl oxygen are effectively stabilized by the central ammonium moiety and the aromatic substituents at the 3,3′-position. The transition state for the *S*-production is disfavored in energy due to the steric hindrance between the phenyl group of the enolate ion and the binaphthyl subunit of the catalyst. Our computational approach has proven useful in finding unknown or unexpected transition structures responsible for enantioselectivity. This work will inspire an in silico design of next-generation asymmetric organocatalysts.

dx.doi.org/10.1021/ol4033545 | *Org. Lett.* 2014, 16, 472−475

■ ASSOCIATED CONTENT

Supporting Information

Two isomers of the enolate ion, superimposed top three conformations, the conformations of the partially optimized structures, benchmark calculations, the N···Br and N···O distances, and *xyz* coordinates of the top 10 conformations (2 figures and 3 tables). This material is available free of charge via the Internet at http://pubs.acs.org.

■ AUTHOR INFORMATION

Corresponding Author

*E-mail: kazunari@ms.ifoc.kyushu-u.ac.jp.

Notes

The authors declare no competing financial interest.

■ ACKNOWLEDGMENTS

We thank Grants-in-Aid for Scientific Research (Nos. 22245028, 24109014, and 24550190) from the Japan Society for the Promotion of Science (JSPS) and the Ministry of Education, Culture, Sports, Science and Technology of Japan (MEXT). We also thank the MEXT Projects of "Integrated Research on Chemical Synthesis" and "Elements Strategy Initiative to Form Core Research Center".

■ REFERENCES

(1) *Phase-Transfer Catalysis*; Halpern, M. E., Ed.; ACS Symposium Series 659; American Chemical Society: Washington, DC, 1997.
(2) O'Donnell, M. J. *Acc. Chem. Res.* **2004**, *37*, 506.
(3) Lygo, B.; Andrews, B. I. *Acc. Chem. Res.* **2004**, *37*, 518.
(4) Cheong, P. H.-Y.; Legault, C. Y.; Um, J. M.; Çelebi-Ölçüm, N.; Houk, K. N. *Chem. Rev.* **2011**, *111*, 5042.
(5) Maruoka, K.; Ooi, T. *Chem. Rev.* **2003**, *103*, 3013.
(6) Hashimoto, T.; Maruoka, K. *Chem. Rev.* **2007**, *107*, 5656.
(7) Ooi, T.; Maruoka, K. *Angew. Chem., Int. Ed.* **2007**, *46*, 4222.
(8) Shirakawa, S.; Maruoka, K. *Angew. Chem., Int. Ed.* **2013**, *52*, 4312.
(9) Ooi, T.; Kameda, M.; Maruoka, K. *J. Am. Chem. Soc.* **2003**, *125*, 5139.
(10) MacroModel, Schrödinger, Inc., http://www.schrodinger.com.
(11) Banks, J. L.; Beard, H. S.; Cao, Y.; Cho, A. E.; Damm, W.; Farid, R.; Felts, A. K.; Halgren, T. A.; Mainz, D. T.; Maple, J. R.; Murphy, R.; Philipp, D. M.; Repasky, M. P.; Zhang, L. Y.; Berne, B. J.; Friesner, R. A.; Gallicchio, E.; Levy, R. M. *J. Comput. Chem.* **2005**, *26*, 1752.
(12) Korth, M. *J. Chem. Theory Comput.* **2010**, *6*, 3808.
(13) Stewart, J. J. P. *Stewart Computational Chemistry*; Colorado Springs, CO, USA, http://OpenMOPAC.net (2012).
(14) Grimme, S. *J. Comput. Chem.* **2006**, *27*, 1787.
(15) Eichkorn, K.; Treutler, O.; Öhm, H.; Häser, M.; Ahlrichs, R. *Chem. Phys. Lett.* **1995**, *240*, 283.
(16) Eichkorn, K.; Weigend, F.; Treutler, O.; Ahlrichs, R. *Theor. Chem. Acc.* **1997**, *97*, 119.
(17) Ahlrichs, R.; Bär, M.; Häser, M.; Horn, H.; Kölmel, C. *Chem. Phys. Lett.* **1989**, *162*, 165.
(18) Schäfer, A.; Horn, H.; Ahlrichs, R. *J. Chem. Phys.* **1992**, *97*, 2571.
(19) Schäfer, A.; Huber, C.; Ahlrichs, R. *J. Chem. Phys.* **1994**, *100*, 5829.
(20) (a) Becke, A. D. *Phys. Rev. A* **1988**, *38*, 3098. (b) Becke, A. D. *J. Chem. Phys.* **1993**, *98*, 5648.
(21) Lee, C.; Yang, W.; Parr, R. G. *Phys. Rev. B* **1988**, *37*, 785.
(22) Vosko, S. H.; Wilk, L.; Nusair, M. *Can. J. Phys.* **1980**, *58*, 1200.
(23) Weigend, F.; Häser, M. *Theor. Chem. Acc.* **1997**, *97*, 331.
(24) Hättig, C.; Weigend, F. *J. Chem. Phys.* **2000**, *113*, 5154.
(25) Kano, T.; Lan, Q.; Wang, X.; Maruoka, K. *Adv. Synth. Catal.* **2007**, *349*, 556.